Analysis of Drosophila Segmentation Network Identifies a JNK Pathway Factor Overexpressed in Kidney Cancer

Author(s): Jiang Liu, Murad Ghanim, Lei Xue, Christopher D. Brown, Ivan Iossifov, Cesar Angeletti, Sujun Hua, Nicolas Nègre, Michael Ludwig, Thomas Stricker, Hikmat A. Al-Ahmadie, Maria Tretiakova, Robert L. Camp, Montse Perera-Alberto, David L. Rimm, Tian Xu, Andrey Rzhetsky and Kevin P. White

Source: *Science*, New Series, Vol. 323, No. 5918 (Feb. 27, 2009), pp. 1218-1222
Published by: American Association for the Advancement of Science
Stable URL: http://www.jstor.org/stable/25471594
Accessed: 29-04-2015 18:42 UTC

Table 1. MIC values for β-lactams in the presence of 2.5 μg ml^{-1} clavulanic acid. The XDR strains were a subset of those previously reported (*18*).

Strain	β-lactam	MIC value (μg ml^{-1})
Erdman	Meropenem	0.5
H37Rv	Amoxicillin	>10
H37Rv	Ampicillin	5.0
H37Rv	Cefotaxime	1.25
H37Rv	Cephalothin	0.94
H37Rv	Imipenem	0.16
H37Rv	Meropenem	0.32
XDR-1	Meropenem	0.94
XDR-2	Meropenem	0.625
XDR-3	Meropenem	0.625
XDR-4	Meropenem	0.625
XDR-5	Meropenem	0.625
XDR-6	Meropenem	0.625
XDR-7	Meropenem	0.625
XDR-8	Meropenem	0.94
XDR-9	Meropenem	1.25
XDR-10	Meropenem	0.47
XDR-11	Meropenem	0.23
XDR-12	Meropenem	0.625
XDR-13	Meropenem	0.32

tuberculosis. Both clavulanate and meropenem are FDA-approved drugs, and both clavulanate and meropenem are sufficiently free of side effects to be approved for pediatric use in children over 3 months old.

References and Notes

1. H. I. Boshoff, C. E. Barry 3rd, *Nat. Rev. Microbiol.* **3**, 70 (2005).
2. N. R. Gandhi *et al.*, *Lancet* **368**, 1575 (2006).
3. A. Fleming, *Br. J. Exp. Pathol.* **10**, 226 (1929).
4. K. Bush, S. Mobashery, *Adv. Exp. Med. Biol.* **456**, 71 (1998).
5. S. T. Cole *et al.*, *Nature* **393**, 537 (1998).
6. A. R. Flores, L. M. Parsons, M. S. Pavelka Jr., *Microbiology* **151**, 521 (2005).
7. J.-E. Hugonnet, J. S. Blanchard, *Biochemistry* **46**, 11998 (2007).
8. F. Wang, C. Cassidy, J. C. Sacchettini, *Antimicrob. Agents Chemother.* **50**, 2762 (2006).
9. L. W. Tremblay, J.-E. Hugonnet, J. S. Blanchard, *Biochemistry* **47**, 5312 (2008).
10. C. J. Easton, J. R. Knowles, *Biochemistry* **21**, 2857 (1982).
11. M. H. Cynamon, G. S. Palmer, *Antimicrob. Agents Chemother.* **24**, 429 (1983).
12. C. Segura, M. Salvado, I. Collado, J. Chaves, A. Coira, *Antimicrob. Agents Chemother.* **42**, 1524 (1998).
13. I. Dincer, A. Ergin, T. Kocagoz, *Int. J. Antimicrob. Agents* **23**, 408 (2004).
14. J. E. Gomez, J. D. McKinney, *Tuberculosis (Edinburgh)* **84**, 29 (2004).
15. Y. Zhang, *Front. Biosci.* **9**, 1136 (2004).
16. M. Lavollay *et al.*, *J. Bacteriol.* **190**, 4360 (2008).
17. L. G. Wayne, L. G. Hayes, *Infect. Immun.* **64**, 2062 (1996).
18. C. Y. Jeon *et al.*, *Clin. Infect. Dis.* **46**, 42 (2008).
19. H. F. Chambers, T. Kocagoz, T. Sipit, J. Turner, P. C. Hopewell, *Clin. Infect. Dis.* **26**, 874 (1998).
20. Materials and methods are available as supporting material on *Science* Online.

21. The authors wish to thank J. Chan and E. Russel for help in the Wayne model studies and H. Xiao for assistance in mass spectrometry. This work was supported partially by the NIH (AI33696 to J.S.B.); in part by the Intramural Research Program of the NIH, National Institute of Allergy and Infectious Diseases; and in part by a grant from the Bill and Melinda Gates Foundation and the Wellcome Trust through the Grand Challenges in Global Health Initiative. A provisional U.S. patent application was filed on 27 May 2008 related to this work. Structure coordinates have been deposited as Protein Data Bank identification code 3DWZ.

Supporting Online Material

www.sciencemag.org/cgi/content/full/323/5918/1215/DC1
Materials and Methods
Figs. S1 to S4
Tables S1 and S2
References

21 October 2008; accepted 6 January 2009
10.1126/science.1167498

Analysis of *Drosophila* Segmentation Network Identifies a JNK Pathway Factor Overexpressed in Kidney Cancer

Jiang Liu,[1,2*] Murad Ghanim,[1,2*†] Lei Xue,[3*] Christopher D. Brown,[1,2] Ivan Iossifov,[1,4‡] Cesar Angeletti,[5] Sujun Hua,[1,2] Nicolas Nègre,[1,2] Michael Ludwig,[1,2,6] Thomas Stricker,[1,2,7] Hikmat A. Al-Ahmadie,[7] Maria Tretiakova,[7] Robert L. Camp,[5] Montse Perera-Alberto,[8] David L. Rimm,[5] Tian Xu,[3] Andrey Rzhetsky,[1,4] Kevin P. White[1,2,6§]

We constructed a large-scale functional network model in *Drosophila melanogaster* built around two key transcription factors involved in the process of embryonic segmentation. Analysis of the model allowed the identification of a new role for the ubiquitin E3 ligase complex factor SPOP. In *Drosophila*, the gene encoding SPOP is a target of segmentation transcription factors. *Drosophila* SPOP mediates degradation of the Jun kinase phosphatase Puckered, thereby inducing tumor necrosis factor (TNF)/Eiger–dependent apoptosis. In humans, we found that SPOP plays a conserved role in TNF-mediated JNK signaling and was highly expressed in 99% of clear cell renal cell carcinomas (RCCs), the most prevalent form of kidney cancer. SPOP expression distinguished histological subtypes of RCC and facilitated identification of clear cell RCC as the primary tumor for metastatic lesions.

Over the last three decades, extensive molecular and genetic analyses have characterized the identity of and interactions between components of the *Drosophila* segmentation process (*1*). Maternal factors distributed in gradients along the anterior-posterior (A-P) axis activate zygotic transcription of gap genes, which encode transcription factors that activate sets of pair-rule genes including the homeobox transcription factors Even-skipped (Eve) and Fushi tarazu (Ftz). These pair-rule proteins then directly regulate segment polarity genes that determine the internal A-P orientation of each segment. Many of the human homologs of these genes and their downstream targets play critical roles in human diseases, especially cancers (*2*, *3*). In an effort to extract new information from the *Drosophila* segmentation network, as well as to mine this network for previously unknown disease-related genes, we built a large-scale predictive network model around Ftz and Eve.

We analyzed gene expression changes between individual wild-type embryos and embryos with null mutations in *ftz* and *eve* (*1*) collected during a developmental time course from 2 hours until 7 hours after egg laying (AEL). By focusing on the effects of Ftz and Eve 2 to 3 hours AEL (early zygotic expression), we found 1310 genes differentially expressed between the *ftz* mutant and wild type, and 1074 genes differentially expressed between the *eve* mutant and wild type (false discovery rate < 0.001; tables S1 and S2).

Using antibodies specific for Ftz or Eve, we performed chromatin immunoprecipitation (ChIP) and mapped genome-wide transcription factor binding in cellular blastoderm embryos 2 hours AEL on custom-designed high-density DNA microarrays (*4*). We found 1286 Ftz- and

1499 Eve-bound probes (intensity $P < 0.0001$ and Z score > 1.96, see supplemental methods; 21 probes on both lists map within 500 base pairs). We analyzed several methods for probe-to-target gene mapping to maximize the overlap between the differentially expressed and ChIP target gene sets (see supplemental methods and fig. S1). The greatest such enrichment was obtained by designating genes within 1 kb of a binding site as targets. At this threshold, we identified 969 Ftz ChIP-chip target genes and 932 Eve ChIP-chip target genes (overlap 175 genes; tables S3 and S4).

Genes both differentially expressed and targeted by ChIP-chip binding site mapping were considered as putative direct target genes. We thus identified 137 Ftz direct target genes (Fig. 1A) and 98 Eve direct target genes (fig. S2; overlap 9 genes). Figure 1A (right) shows the locations of binding sites at Ftz or Eve direct target genes. Analysis of direct target gene annotations indicates that 39 genes (21%) regulate transcription and 74 genes (40%) are involved in developmental processes (Fig. 1A, center); both annotation classes were significantly enriched compared to the 9.6% and 18% of *Drosophila* genes annotated as transcriptional or developmental regulators, respectively ($P = 1.05 \times 10^{-6}$ and $P = 1.81 \times 10^{-12}$; hypergeometric test). A complete target list can be found in tables S5 and S6.

To extend our Ftz-Eve network model beyond direct transcriptional regulation, we included automated literature-mining methods to capture published interactions of target genes (*5*). We then integrated yeast two-hybrid–based protein-protein interaction data (*6*) into our model by connecting protein interactions between existing components in the network. To limit the size of the network, we extended the protein-protein interaction only one degree from the direct targets of Ftz or Eve. The resulting Ftz-Eve regulatory network model included 4084 genes/proteins and 6648 interactions between them (fig. S3).

To confirm parts of the network model topology, we examined several genes that are expressed in segmental patterns (*7*) and validated a limited set of interactions by genetic and biochemical testing of simple predictions from our network model (fig. S4). Analysis of the Eve-Ftz network identified 150 different genes as direct targets of Eve or Ftz that also have unambiguous human homologs. From this gene set, we identified a top candidate, *CG9924* or *roadkill* (*rdx*), which ranks first in network betweenness-centrality and thus constitutes a major network hub (*8*) (see supplemental methods and table S8). The *rdx* gene encodes a BTB domain protein that has been shown to regulate Cubitus interruptus (Ci) degradation in the Hedgehog pathway (*9*, *10*). This product of the *rdx* gene is 79% identical to the human protein SPOP, and these proteins appear to be orthologs (fig. S5) (*9*, *10*); we refer to the *rdx* gene product(s) as *Drosophila* SPOP (D-SPOP).

Our network model indicates that the *D-SPOP* gene is a direct target of Ftz at 2 to 3 hours AEL and that the D-SPOP protein interacts with the Jun kinase phosphatase Puckered (Puc) (Fig. 1B). RNA in situ hybridizations for *D-SPOP* mRNA in *ftz* mutant embryos confirmed that *ftz* is indeed required for *D-SPOP* expression in parasegments that normally express Ftz (Fig. 1C). We did not observe significant misexpression of *D-SPOP* mRNA in *eve* mutant embryos at 2 to 3 hours AEL (fig. S6), suggesting that the Ftz effects on *D-SPOP* mRNA expression occur before the Eve effect. We found that the D-SPOP protein segmental expression pattern was completely lost in *eve* mutant embryos at 6 to 7 hours AEL (Fig. 1D), similar to the expression pattern observed for the well-characterized Ftz and Eve target gene *engrailed* (*11*, *12*). Previous studies also indicate that D-SPOP is regulated by Hedgehog (Hh) later in development, indicating another layer of D-SPOP regulation by the segment polarity system

[1]Institute for Genomics and Systems Biology, The University of Chicago and Argonne National Laboratory, Chicago, IL 60637, USA. [2]Department of Human Genetics, The University of Chicago, Chicago, IL 60637, USA. [3]Howard Hughes Medical Institute, Department of Genetics, Yale University School of Medicine, New Haven, CT 06519, USA. [4]Department of Medicine, The University of Chicago, Chicago, IL 60637, USA. [5]Department of Pathology, Yale University School of Medicine, New Haven, CT 06520, USA. [6]Department of Ecology and Evolution, The University of Chicago, Chicago, IL 60637, USA. [7]Department of Pathology, The University of Chicago, Chicago, IL 60637, USA. [8]Department of Anatomy, La Laguna University, La Laguna, 38320 Tenerife, Spain.

*These authors contributed equally to this work.
†Present address: Department of Entomology, The Volcani Center, Bet Dagan, Israel.
‡Present address: Cold Spring Harbor Laboratory, One Bungtown Road, P.O. Box 100, Cold Spring Harbor, NY 11742, USA.
§To whom correspondence should be addressed. E-mail: kpwhite@uchicago.edu

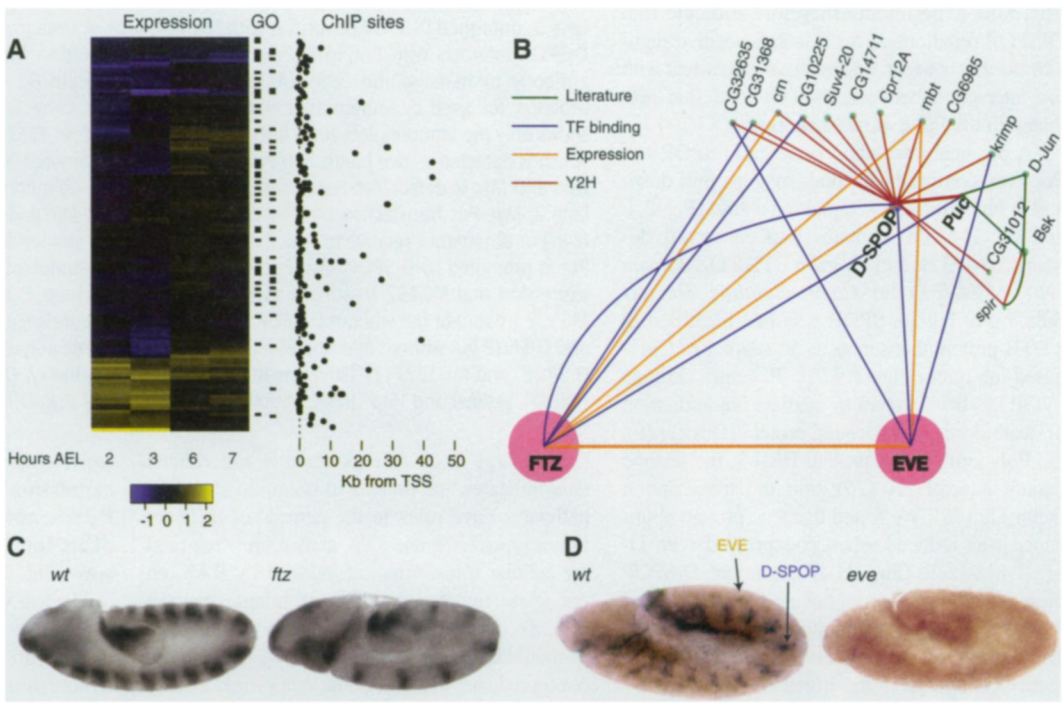

Fig. 1. *Drosophila* segmentation network. **(A)** Identification of direct targets of Ftz. (Left) Heat map depicts $\log_2$-fold change in gene expression of mutant versus wild type. Columns represent time points in hours after egg laying (AEL). Rows depict individual genes, sorted by hierarchical clustering. (Center) Genes involved in regulation of development (left tick marks) or transcriptional regulation (right tick marks) from gene ontology (GO) annotations. (Right) Locations of binding sites relative to the transcription start site of each gene. **(B)** Detailed D-SPOP subnetwork showing that D-SPOP is regulated by FTZ and EVE and interacts with puc. **(C)** RNA in situ hybridization of D-SPOP in wild-type and *ftz* mutant backgrounds. Fourteen and 7 stripes of expression were observed in wild-type and *ftz* embryos, respectively. **(D)** Staining with antibodies specific for D-SPOP and EVE in wild-type and *eve* mutant backgrounds. D-SPOP [BCIP-NBT (bromochloroindolyl phosphate–nitro blue tetrazolium), blue] was stained in segmental grooves in wild type, but all expression was lost in *eve* mutant embryos. Eve (diaminobenzidine, brown) was stained in neurons.

(*9*). Together, these data strongly indicate that *D-SPOP* expression is downstream of the pair-rule genes in the segmentation hierarchy.

Knockdown of *D-SPOP* mRNA expression by RNA interference (RNAi) and P-element insertion mutagenesis of the *D-SPOP* gene resulted in severe and consistent disruption of both the peripheral and the central nervous system (CNS) (fig. S7). Such phenotypes are recapitulated by mutating *ftz* or *eve* and are likely due to mid-embryonic functions of D-SPOP when Ftz and Eve become active in the CNS (*13*, *14*). Furthermore, it was recently demonstrated that the *Drosophila* Eiger/TNF (tumor necrosis factor) pathway regulates embryonic neuroblast division (*15*). Thus, we hypothesized that the function of D-SPOP in nervous tissue development may result from its interaction with Puc, which mediates a feedback loop by negatively regulating *basket* (*Drosophila* JNK) in the *Drosophila* Eiger/TNF pathway (*16*) (Fig. 1B).

In *Drosophila*, ectopic expression of Eiger in neuronal cells in the developing eye induces apoptosis through the JNK pathway, resulting in a reduced adult eye size (Fig. 2, A and B) (*17*). Deletion of one wild-type copy of *D-SPOP* or RNAi knockdown of *D-SPOP* mRNA partially suppresses the eye phenotype of Eiger expression (Fig. 2, C and D). Additionally, ectopic expression of D-SPOP in the developing eyes produces a small and rough eye phenotype (Fig. 2E). Analysis of genetic interactions between the genes encoding D-SPOP and other members of the Eiger-JNK pathway (fig. S8) indicates that D-SPOP is acting downstream of dTAK1 (JNKKK) and Hep (JNKK) and upstream of Bsk (JNK) and Puc. Our experiments therefore indicate that D-SPOP functions as an essential positive regulator for Eiger-triggered apoptosis, consistent with the interaction between D-SPOP and Puc predicted in the Ftz-Eve network model.

A physical interaction between D-SPOP and Puc was confirmed by both in vitro pull-down and in vivo immunoprecipitation assays (Fig. 2, F and G). D-SPOP contains two conserved domains, a MATH domain and a BTB/POZ domain (*18*). MEL-26, the *Caenorhabditis elegans* ortholog of human SPOP, was first identified as a BTB protein that serves as an adaptor of Cul3-based ubiquitin ligase (*18*). Recently, human SPOP has been shown to mediate ubiquitination of death domain–associated protein (Daxx) (*19*), the Polycomb group protein BMI-1, the histone variant MacroH2A (*20*), and the transcription factor Gli (*10*). We found that Puc protein abundance was reduced when coexpressed with D-SPOP in S2 cells (Fig. 2H). Furthermore, D-SPOP promoted Puc ubiquitination in S2 cells treated with the proteasome inhibitor MG132 (Fig. 2I). Together, these results indicate that D-SPOP induces apoptosis in the Eiger/TNF pathway by mediating Puc ubiquitination and degradation (Fig. 2J).

Homologs of several Ftz and Eve targets have been shown to be involved in human cancers

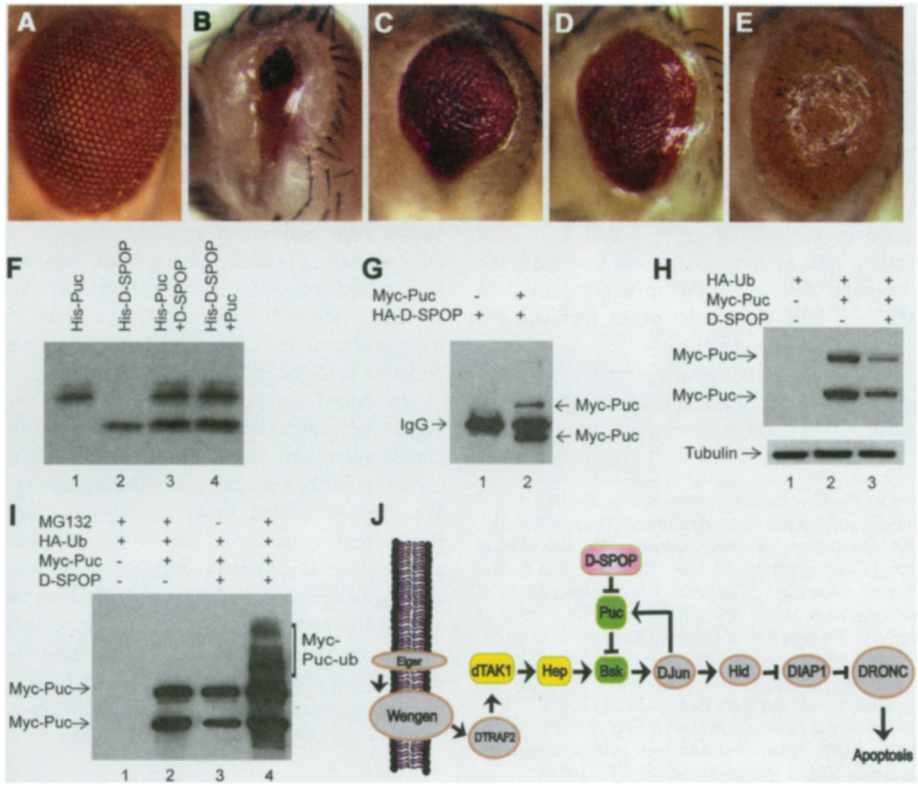

Fig. 2. D-SPOP promotes puc ubiquitination and degradation. (**A**) Light micrographs of *Drosophila* adult eyes for wild-type (*GMR-Gal4/+*). (**B**) Egr triggered cell death and produced a small eye phenotype (*GMR-Gal4; UAS-Egr/+*). (**C**) Deleting one copy of *D-SPOP* (*GMR-Gal4; UAS-Egr/+; D-SPOPΔ6/+*) suppressed the phenotype of (*GMR-Gal4; UAS-Egr/+*). (**D**) Coexpression of *D-SPOP-RNAi* (*GMR-Gal4; UAS-Egr/+; UAS-D-SPOP-RNAi*) suppressed the phenotype of (*GMR-Gal4; UAS-Egr/+*). (**E**) Expression of D-SPOP (*GMR-Gal4; UAS-D-SPOP/+*) produced rough eyes with slightly reduced size. (**F**) D-SPOP interacts with Puc in an in vitro affinity assay. Proteins were translated in vitro, purified on a nickel-ion (Ni^{2+}) column, and detected by Western blot (see supplementary methods). Lane 1, His-Puc; lane 2, His-D-SPOP; lane 3, untagged D-SPOP copurifies with His-Puc; lane 4, untagged Puc copurifies with His-D-SPOP. (**G**) D-SPOP interacts with Puc in an in vivo immunopreciptation (IP) assay. IPs were carried out with an antibody to hemagglutin (anti-HA) using cell lysates from S2 cells expressing the indicated fusion proteins, followed by immunoblot with anti-Myc epitope. Lane 1, IP of HA-D-SPOP control transfection shows only the immunoglobulin G (IgG) band; lane 2, IP of HA-D-SPOP in cells cotransfected with Myc-Puc, which is detected as two bands. (**H**) Puc degradation is promoted by SPOP. Western blots were performed with anti-Myc to detect Myc-Puc fusion protein. Lane 1, HA-ubiquitin (HA-Ub) transfection negative control; lane 2, Myc-Puc transfection positive control; lane 3, Myc-Puc and D-SPOP cotransfection shows reduced Myc-Puc abundance relative to lane 2. Tubulin is detected as a loading control. (**I**) In vivo ubiquitination of Puc is promoted by D-SPOP. Myc-Puc was detected by immunoblot with anti-Myc epitope. Lane 1, HA-Ub expression and MG132 treatment as a negative control; lane 2, HA-Ub and Myc-Puc coexpression with MG132 treatment but without D-SPOP; lane 3, Myc-Puc abundance decreased with coexpression of HA-Ub and D-SPOP but without addition of MG132; lane 4, Myc-Puc polyubiquitination in the presence of HA-Ub, D-SPOP, and MG132. (**J**) TNF/Eiger-induced apoptosis pathway. D-SPOP (pink) is downstream of dTAK1 (JNKKK, yellow) and Hep (JNKK, yellow), and upstream of Bsk (DJNK, green) and Puc (MKP, green).

(*21*); a large body of experimental and clinical data indicates that defects in ubiquitin signaling pathways have roles in the genesis of different tumor types (*22*); and JNK activation is required for cellular transformation induced by RAS, an oncogene mutated in 30% of human cancers (*23*). To determine whether human SPOP's role in modulating TNF-stimulated JNK signaling is conserved, we treated human embryonic kidney 293 (HEK293) cells overexpressing SPOP with TNF-α, then analyzed the abudance of phosphorylated JNK (P-JNK) and phosphorylated c-Jun (P-c-Jun). Consistent with its role in *Drosophila* as an activator of the pathway, overexpression of SPOP increases the amount of P-JNK and P-c-Jun, indicating conservation of its function in modulating the JNK pathway (Fig. 3A).

To test whether SPOP is associated with human cancers, we screened SPOP protein abundance with tissue microarrays that contained 20 tumors from each of 18 different organs. We found that 85% of renal cell carcinomas (RCCs) showed high expression of SPOP, whereas normal kidney tissue was uniformly negative (Fig. 3B and Table 1). To further investigate the potential

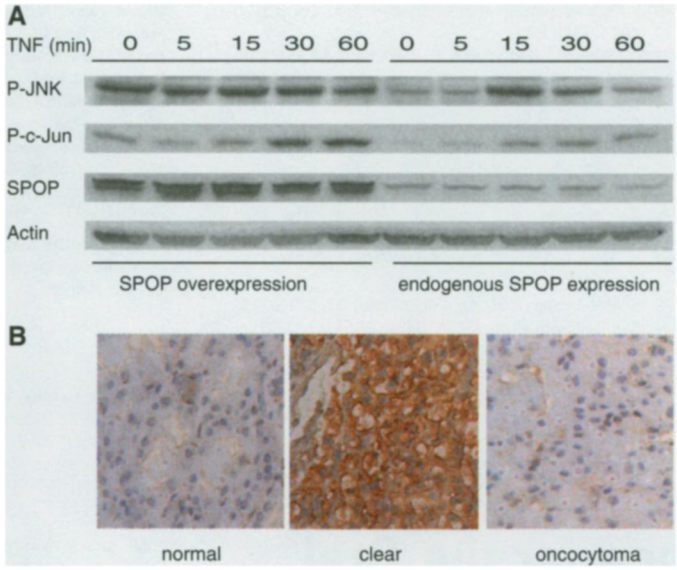

Fig. 3. Function of SPOP in the mammalian TNF pathway and overexpression in RCC. (**A**) Overexpression of SPOP increases the abundance of P-JNK and P-c-Jun. HEK293 cells were transfected with SPOP and then treated with TNF (50 ng/ml) at 0, 5, 15, 30, 60 min, followed by immunoblotting. In control treatments, HEK293 cells were transfected with empty pcDNA3.1 vector, and thus only express endogenous amounts of SPOP. (**B**) SPOP expression in RCC tissue. Tissue images are from normal kidney, oncocytoma, and clear cell renal carcinoma. A SPOP-specific monoclonal antibody (SPOP-5G) was used to detect SPOP expression in tissue (diaminobenzidine, brown staining).

Table 1. Tissue microarray screening for SPOP expression in 18 cancer types from different organs. SPOP is highly expressed in RCC as compared to normal renal tissue. Endometrial carcinoma and germ-cell tumors also display higher SPOP staining relative to comparable normal tissues.

Tissue type	Normal tissue	Cancer tissue
Kidney/renal	5 negative	17 positive; 3 negative
Uterus/endometrial	5 negative	10 positive; 4 negative
Testis/germ cell	5 weak	18 positive; 2 negative
Soft tissue/sarcoma	5 negative	20 weak or negative
Lung	5 weak	20 weak
Bladder	5 weak or negative	20 weak or negative
Breast	5 weak or negative	20 weak or negative
Prostate	5 negative	1 positive; 19 negative
Pancreas	5 negative	20 negative
Lymphoma	5 negative	19 weak or negative
Thyroid	5 negative	20 weak or negative
Colon	5 negative	20 negative
Ovary	5 weak or negative	20 weak or negative
Skin/melanoma	5 weak or negative	20 weak or negative
Liver	5 positive	7 positive; 13 negative
Skin/squamous	5 weak or negative	20 weak or negative
Brain	5 weak or negative	20 weak or negative
Stomach/gastric	5 weak or negative	20 weak or negative

of SPOP as a marker, we designed a large tissue array containing more than 300 RCC samples. Of the tumor samples, 77% were positive for SPOP staining; normal kidney samples were all negative (Table 2).

RCC is a heterogeneous group of tumors with distinct histological subtypes, including clear cell, papillary, chromophobe, and other rare subtypes in addition to oncocytoma, which is a benign solid renal tumor (*24*). Most RCCs (up to 75%) are of the clear cell type and can be subtyped by hematoxylin and eosin staining morphology, but diagnostic difficulties arise when clear cell RCCs display morphologic features that overlap with those of other RCC subtypes and nonrenal tumors (*25*–*27*). At present, a panel of immunohistochemical markers is used to differentiate the major subtypes of RCC in difficult cases (*26*, *27*). Unfortunately, these panels lack a specific and sensitive marker that is positive in clear cell RCC (*26*, *27*). Recently, carbonic anhydrase IX has been proposed as a positive marker for clear cell RCC, but it is positive in other RCCs and several other tumor types as well (*28*–*30*). Patient tumor samples in our studies were classified into different types according to the recent World Health Organization classification system. We found that 99% of the clear cell RCCs and 86% of the chromophobe RCCs showed positive staining for SPOP, but only 22% of papillary-type RCCs were SPOP positive. Four out of 31 papillary RCCs from the general pathology reports were shown to be misdiagnosed as clear cell RCCs when

Table 2. SPOP expression in RCCs. RCC tissue sections were analyzed by staining with SPOP-specific monoclonal antibody (SPOP-5G). Patient samples are classified into different categories depending on cell type.

Renal cell type	Positive	Negative
Clear cell	179	1
Chromophobe	6	1
Papillary	6	21
Oncocytic	2*	28
Rare type	6	8
Total tumor	199	59
Normal tissue	0	295

*Both cases are weak staining.

Table 3. SPOP expression in metastatic lesions where RCCs were the primary tumors. Metastatic tissues were analyzed by staining with SPOP-specific monoclonal antibody (SPOP-5G). Patient samples are classified into different categories depending on cell type of the primary tumor.

Primary RCC type	Positive	Negative
Clear cell	71	2
Chromophobe	3	1
Papillary	1	2
Rare type	3	4

the tumor biopsies were reanalyzed by urological pathologists. All four of these misdiagnosed RCCs have papillary architecture and were subsequently shown to stain positive for SPOP. Our tissue array also included benign oncocytomas, which can mimic RCC both clinically and pathologically, in turn potentially subjecting patients to unnecessary surgeries and additional morbidities. Only 6% of oncocytomas showed weak positive staining. These results indicate that SPOP is a highly sensitive and specific diagnostic biomarker for clear cell RCC and can help distinguish histological subtypes of RCC.

Up to 30% of RCC patients present with metastases; half of the rest will develop metastases later in their course, 90% of which are clear cell RCCs. Accordingly, we further screened for SPOP staining in confirmed metastases from RCC and found that 97% of them were positive (Table 3), indicating that SPOP may be a useful biomarker to identify clear cell RCC as the site of the primary tumors in cases of metastases of unknown origin. Together, our results demonstrate that novel functions for conserved molecules can readily be extracted from data mining of large-scale networks in *Drosophila* and provide a strategy for rapid identification of factors that may have clinical relevance as biomarkers or drug targets for human diseases.

References and Notes

1. A. Nasiadka, B. H. Dietrich, H. M. Krause, in *Advances in Developmental Biology and Biochemistry*, M. DePamphilis, Ed. (Elsevier, Amsterdam, 2002), vol. 12, p. 155.
2. S. A. Hahn *et al.*, *Science* **271**, 350 (1996).

3. R. L. Johnson *et al.*, *Science* **272**, 1668 (1996).
4. V. Stolc *et al.*, *Science* **306**, 655 (2004).
5. A. Rzhetsky *et al.*, *J. Biomed. Inform.* **37**, 43 (2004).
6. L. Giot *et al.*, *Science* **302**, 1727 (2003).
7. P. Tomancak *et al.*, *Genome Biol.* **8**, R145 (2007).
8. H. Jeong, S. P. Mason, A. L. Barabasi, Z. N. Oltvai, *Nature* **411**, 41 (2001).
9. D. Kent, E. W. Bush, J. E. Hooper, *Development* **133**, 2001 (2006).
10. Q. Zhang *et al.*, *Dev. Cell* **10**, 719 (2006).
11. K. Harding, C. Rushlow, H. J. Doyle, T. Hoey, M. Levine, *Science* **233**, 953 (1986).
12. J. B. Jaynes, M. Fujioka, *Dev. Biol.* **269**, 609 (2004).
13. C. Q. Doe, Y. Hiromi, W. J. Gehring, C. S. Goodman, *Science* **239**, 170 (1988).
14. J. Broadus *et al.*, *Mech. Dev.* **53**, 393 (1995).
15. H. Wang, Y. Cai, W. Chia, X. Yang, *EMBO J.* **25**, 5783 (2006).
16. E. Martin-Blanco *et al.*, *Genes Dev.* **12**, 557 (1998).
17. T. Igaki *et al.*, *EMBO J.* **21**, 3009 (2002).
18. L. Xu *et al.*, *Nature* **425**, 316 (2003).
19. J. E. Kwon *et al.*, *J. Biol. Chem.* **281**, 12664 (2006).
20. I. Hernandez-Munoz *et al.*, *Proc. Natl. Acad. Sci. U.S.A.* **102**, 7635 (2005).
21. C. J. Potter, G. S. Turenchalk, T. Xu, *Trends Genet.* **16**, 33 (2000).
22. D. Hoeller, C. M. Hecker, I. Dikic, *Nat. Rev. Cancer* **6**, 776 (2006).
23. C. Weiss, D. Bohmann, *Cell Cycle* **3**, 111 (2004).
24. H. T. Cohen, F. J. McGovern, *N. Engl. J. Med.* **353**, 2477 (2005).
25. J. Rosai, *Rosai and Ackerman's Surgical Pathology* (Mosby, New York, ed. 9, 2004).
26. B. F. Skinnider, M. B. Amin, *Semin. Diagn. Pathol.* **22**, 51 (2005).
27. M. Zhou, A. Roma, C. Magi-Galluzzi, *Clin. Lab. Med.* **25**, 247 (2005).
28. H. A. Al-Ahmadie *et al.*, *Am. J. Surg. Pathol.* **32**, 377 (2008).
29. B. C. Leibovich *et al.*, *J. Clin. Oncol.* **25**, 4757 (2007).
30. C. Potter, A. L. Harris, *Cell Cycle* **3**, 164 (2004).
31. We thank J. Jiang, M. Van Lohuizen, C. Chung, D. McEwen for providing expression vectors. Microarray data described in this paper have been deposited in the NCBI Gene Expression Omnibus (GEO) under accession code GSE14086 (expression data) and GSE14289 (ChIP data).

M.G. was supported by Vaadia-BARD Postdoctoral Fellowship Award No. FI-315-2001 from BARD, The United States–Israel Binational Agricultural Research and Development Fund. C.D.B was supported by a Lilly Life Science Research Fellowship. This work was supported by grants from the W. M. Keck Foundation, the Arnold and Mabel Beckman Foundation, and the Searle Funds at The Chicago Community Trust from the Chicago Biomedical Consortium to K.P.W.

Supporting Online Material

www.sciencemag.org/cgi/content/full/1157669/DC1
Materials and Methods
Figs. S1 to S8
Tables S1 to S8
References

12 March 2008; accepted 14 January 2009
Published online 22 January 2009;
10.1126/science.1157669
Include this information when citing this paper.

In Bad Taste: Evidence for the Oral Origins of Moral Disgust

H. A. Chapman,[1]* D. A. Kim,[1] J. M. Susskind,[1] A. K. Anderson[1,2]*

In common parlance, moral transgressions "leave a bad taste in the mouth." This metaphor implies a link between moral disgust and more primitive forms of disgust related to toxicity and disease, yet convincing evidence for this relationship is still lacking. We tested directly the primitive oral origins of moral disgust by searching for similarity in the facial motor activity evoked by gustatory distaste (elicited by unpleasant tastes), basic disgust (elicited by photographs of contaminants), and moral disgust (elicited by unfair treatment in an economic game). We found that all three states evoked activation of the levator labii muscle region of the face, characteristic of an oral-nasal rejection response. These results suggest that immorality elicits the same disgust as disease vectors and bad tastes.

Although rationalist theories of moral psychology have long emphasized the role of conscious reasoning in morality (*1*, *2*), recent empirical (*3*–*5*) and theoretical (*6*, *7*) work suggests that emotion may also play a key role in moral judgment. These newer theories make the claim that moral cognition relies primarily on phylogenetically older affective systems, rather than on more recently evolved higher cognitive functions (*6*, *7*). For example, it has been proposed that the violation of moral norms might evoke a kind of moral revulsion or disgust in victims or onlookers (*8*–*10*). Disgust is a somewhat surprising candidate for a moral emotion, given its hypothesized origins in the very concrete, nonsocial, and straightforwardly adaptive functions of rejecting toxic or contaminated food and avoiding disease (*8*). In the moral domain, this rejection impulse might have been co-opted to promote withdrawal from transgressors, or even from the thought of committing a transgression. If the primitive motivational system of disgust is indeed activated by abstract moral transgressions, it would provide strong support for the idea that the human moral sense is built from evolutionarily ancient precursors.

The notion that moral transgressions might evoke the same disgust as potential toxins and disease agents has not gone unchallenged, however. Some have argued that just as a "thirst" for knowledge does not denote a desire to drink, moral "disgust" may reflect not the engagement of more primitive forms of disgust but merely the use of a compelling metaphor for socially offensive behavior (*11*, *12*). As well, prominent theories of disgust have proposed that although moral disgust may be related to contamination-based disgust (typically evoked by potential disease vectors), it is distinct from the most primitive forms of disgust related to the ingestion of potential toxins, having differentiated from the ancient oral distaste response rooted in chemical sensory rejection (*13*). Thus, the "bad taste" of moral disgust may serve as an abstract metaphor rather than reflect a concrete origin in oral distaste.

The evidence that does exist for the specific involvement of disgust in morality is also problematic. Moral transgressions elicit negative emotions (*9*), and induction of negative emotions such as disgust heightens sensitivity to moral transgressions (*5*). However, these studies do not specifically implicate disgust versus other negative emotions such as anger, nor do they demonstrate that moral "disgust" arises from oral disgust. As well, verbal reports of "disgust" in response to moral transgressions are suspect, because the word "disgusting" is used in colloquial English to describe angering or irritating situations (*14*). Thus, verbal self-report measures of subjective experience alone are not diagnostic of disgust. With respect to neural data, moral transgressions sometimes activate the insula (*10*, *15*), which has also been associated with oral disgust (*16*, *17*). However, many affective and cognitive functions besides disgust are associated with activation of the insula, including anger (*18*), anxiety (*19*), general viscerosensory awareness (*19*), and uncertainty (*20*).

The aim of the current series of studies was to provide a more powerful and direct test of the alleged involvement of disgust in morality, and hence of the notion that moral cognition calls on a phylogenetically older motivational system originating in the rejection of hazardous food. We tested the relationship among simple chemosensory distaste, basic forms of contamination-related disgust, and moral disgust by examining subjective experiential reports and objective facial motor activity associated with these states. Recent work supports Darwin's thesis (*21*) that the configuration of emotional facial expressions has evolved from a functional role in regulating sensory intake (*22*). These ancestral configurations may later have proven useful as social signals, assuming a new function without needing to change their basic form (*21*, *22*). Consequently, if moral disgust really is born from the same emotion involved in rejection of hazardous foods, then there should be continuity in facial actions between moral and oral disgust, despite the former being far removed from its purported origin in food rejection. Because moral disgust might result in subtle overt facial movements reflecting the residual engagement of a primitive oral disgust motor program, we recorded facial motor activity with electromyography (EMG), which enables greater sensitivity in detection relative to visual scoring techniques (*23*).

Our first goal was to collect objective measurements of the basic disgust expression with which to compare the moral disgust expression. The most

[1]Department of Psychology, University of Toronto, Toronto, Ontario M5S 3G3, Canada. [2]Rotman Research Institute, Baycrest Centre for Geriatric Care, Toronto, Ontario M6A 2E1, Canada.

*To whom correspondence should be addressed. E-mail: hanah@aclab.ca (H.A.C.); anderson@psych.utoronto.ca (A.K.A.)